PROGRESS REVIEWS

Graphene devices based on laser scribing technology

Japanese Journal of Applied Physics **57**, 04FA01 (2018)
https://doi.org/10.7567/JJAP.57.04FA01

PROGRESS REVIEW

Graphene devices based on laser scribing technology

Yan-Cong Qiao†, Yu-Hong Wei†, Yu Pang, Yu-Xing Li, Dan-Yang Wang, Yu-Tao Li, Ning-Qin Deng, Xue-Feng Wang, Hai-Nan Zhang, Qian Wang, Zhen Yang, Lu-Qi Tao, He Tian*, Yi Yang*, and Tian-Ling Ren*

Institute of Microelectronics and Tsinghua National Laboratory for Information Science and Technology (TNList), Tsinghua University, Beijing 100084, China

*E-mail: tianhe88@tsinghua.edu.cn; yiyang@tsinghua.edu.cn; RenTL@tsinghua.edu.cn
†These authors contributed equally to this work.

Received October 3, 2017; accepted November 2, 2017; published online February 22, 2018

Graphene with excellent electronic, thermal, optical, and mechanical properties has great potential applications. The current devices based on graphene grown by micromechanical exfoliation, chemical vapor deposition (CVD), and thermal decomposition of silicon carbide are still expensive and inefficient. Laser scribing technology, a low-cost and time-efficient method of fabricating graphene, is introduced in this review. The patterning of graphene can be directly performed on solid and flexible substrates. Therefore, many novel devices such as strain sensors, acoustic devices, memory devices based on laser scribing graphene are fabricated. The outlook and challenges of laser scribing technology have also been discussed. Laser scribing may be a potential way of fabricating wearable and integrated graphene systems in the future.

1. Introduction

Graphene is a two-dimensional material with excellent properties such as ultrahigh mobility,[1,2] thermal conductivity,[3,4] Young's modulus,[5] transparency,[6] a large surface area,[7] and many other unique properties.[1,8,9] Therefore, much attention has been focused on graphene since it was discovered in 2004.[1] Owing to its outstanding properties, graphene has been used to fabricate many devices, such as transistors,[10–13] photodetectors,[14–22] light-emitting diodes,[23,24] transparent and flexible electrodes,[25–28] energy devices,[29–31] mechanics sensors,[32–34] gas sensors,[35,36] resistive random access memories (RRAMs),[37–40] nanogenerators,[41,42] flexible heaters,[43–45] and acoustic devices.[46–49] Besides graphene, many other two-dimensional materials were also discovered, resulting in a complete two-dimensional system.[50] Hexagonal boron nitride (hBN) is a two-dimensional insulator, which is usually used as the dielectric and protective layer for two-dimensional devices.[51,52] Two-dimensional semiconductor transition metal dichalcogenide and black phosphorus have great potential for use in photodetectors[53,54] and transistors.[55,56]

Many methods have been proposed to produce graphene. CVD is a common method of growing high-quality and large-area graphene. Recently, Xu et al. have grown meter-sized single-crystal graphene on industrial Cu foil with in 20 min.[57] However, the cost of CVD is high and the time of the total multistep process including annealing, growth, and cooling is long. In addition, CVD-grown graphene is vulnerable in the follow-up patterning and etching processes. Other methods such as the micromechanical exfoliation and thermal decomposition of silicon carbide are also inefficient. Apart from growing graphene directly, graphene can also be produced by reducing graphene oxide (GO), which is a low-cost and efficient method of producing graphene. After GO reduction, the Young's modulus of reduced graphene oxide (rGO) can be as high as 0.25 TPa.[58] GO can be reduced to graphene by thermal reduction,[59,60] chemical reduction,[61,62] and other methods.[63,64] Among these methods, laser-scribed reduction is a novel method of transferring GO into rGO.[65] $10 \times 10\,cm^2$-size patterned laser-scribed graphene (LSG) can be produced with in 30 min or less without a shield mask,[66] as discussed carefully below.

In this review, we will discuss the fabrication processes and potential applications of LSG. Up to now, laser scribing has been used to develop the whole system, which consists of fabrication, patterning, and the use of devices and integrated systems, as shown in Fig. 1. In Sect. 2, we will introduce some fabrication techniques based on laser scribing in detail. Then, we will present some novel applications based on LSG such as strain sensors,[67] acoustic devices,[68,69] and memory devices[70] contributed by us and other research groups in Sect. 3. The challenges and outlook of LSG system will be discussed in Sect. 4. In Sect. 5, a brief summary of LSG will be given.

2. Laser scribing technology

The thermal atomic force microscopy (AFM) probe was used to partially convert GO to rGO in order to obtain nanoscale graphene patterns.[71] rGO patterns could be 12 nm in width. Owing to the limited scanning range of AFM probes, it was difficult to fabricate large-area rGO by this approach. However, this work enlightened researchers to find another efficient method of patterning rGO, for example laser scribing. Actually, laser-scribed reduction is considered as thermal reduction. It is a novel heating process with its own advantages. Exactly 100 years has been passed since lasers were proposed.[72] In 2010, Zhang et al. used femtosecond lasers for the reduction of GO for the first time.[73] Besides femtosecond lasers,[73–75] other types of laser such as nanosecond,[74] Nd:YAG,[76] Nd:YVO_4,[77] KrF,[78–80] CO_2,[81–85] diode,[86,87] and fiber lasers,[86] and digital versatile disc (DVD) burners[31,35,66,88,89] have also been used to pattern and fabricate graphene.[90] Some metal materials such as silver, copper, iron, and manganese can also be patterned by laser scribing technique.[91]

Unlike conventional two-dimensional materials, rGO has a three-dimensional structure consisting of two-dimensional layer building blocks. During the reduction, the oxygen-containing functional group is transferred to oxygen. The gas is released out of rGO, which makes the distance between graphene layers larger. Therefore, many porous structures are

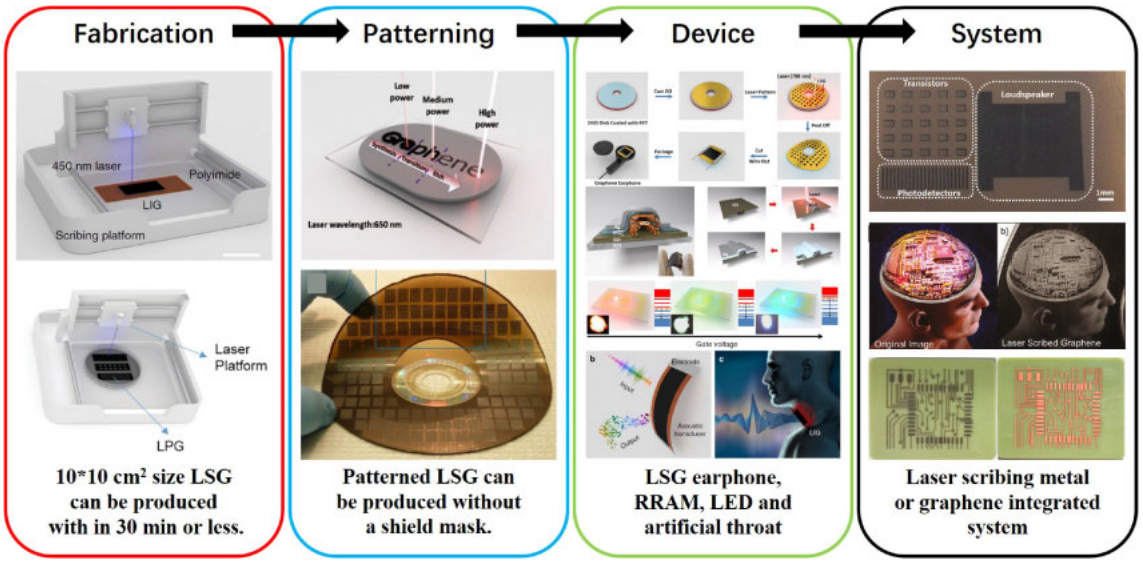

Fig. 1. (Color online) Schematic illustration of laser scribing fabrication, patterning, devices, and system. The figures in the diagram are modified with permission from Ref. 68 © 2017 Nature Publishing Group, Ref. 67 © 2017 Royal Society of Chemistry, Ref. 95 © 2016 Elsevier, Ref. 89 © 2013 Nature Publishing Group, Ref. 69 © 2014 American Chemical Society, Ref. 70 © 2014 American Chemical Society, Ref. 23 © 2015 Nature Publishing Group, Ref. 66 © 2014 Nature Publishing Group, Ref. 35 © 2012 American Chemical Society, and Ref. 100 © 2016 American Chemical Society.

formed. Up to now, two-dimensional materials have not been utilized on a large scale. There is a complementary need to controllably assemble two-dimensional materials into three-dimensional architectures. Shehzad et al. introduced three-dimensional structures based on two-dimensional materials such as graphene, MoS_2, and BN systematically.[92] Such three-dimensional structures can be used as Li-ion batteries, supercapacitors, sensors, and many other devices when composed of other materials such as metals, metal oxides, polymers, and carbon materials.

2.1 Laser scribing graphene based on GO

Graphene can be produced by reducing GO. GO is a complex material, which has a large number of functional groups such as hydroxyl, carbonyl, and carboxyl. Owing to these functional groups, GO can be solved in water easily, differently from graphene. The GO aqueous solution is usually produced by the Hummers method.[93] After multistep redox reaction, graphite powders are converted to the GO aqueous solution. The oxygen content can be judged by the color of GO. The surface wettability and optical and electric properties of GO thin films can be adjusted by UV light irradiation.[94]

Tian et al. realized the wafer-level integration of graphene-based electronic, optoelectronic, and electroacoustic devices by the laser scribing of GO shown in Figs. 2(a) and 2(b).[66] A poly(ethylene terephthalate) (PET) film layer was first attached to a DVD disc. GO dispersion in water at 2 mg mL^{-1} concentration was drop-casted on the surface of the PET film layer; after drying it overnight under ambient condition, the GO film was converted into graphene using 788 nm laser pulses of 5 mW maximum power produced by a commercial DVD burner [Fig. 2(c)]. The electrical conductivity was tuned by changing the oxygen content of rGO. Therefore, by increasing the number of times of laser scribing, the resistance was decreased successively. For example, the initial resistance of the GO film was 580 MΩ. After one, two, and three times of laser scribing, the resistances of rGO thin films were 8.2, 4.8, and 2.3 kΩ, respectively. From the scanning electron microscopy (SEM) images shown in Figs. 2(d)–2(f), the original thickness of GO was 1 μm and the thickness of rGO after scribing was about 10 μm, indicating that the film thickness increased tenfold. However, Joule heat was generated on the surface of GO by the laser, which formed a downward thermal gradient. The amount of Joule heat decreased with the downward diffusion, so the Joule heat was not enough to convert the bottom GO into rGO. Only the surface of GO (about 20 layers) was converted into rGO, rather than the whole 1-μm-thick GO system.

Deng et al. reported a universal method based on one-step laser scribing technology for the rapid synthesis and patterning of large-scale multilayer graphene films.[95] A GO dispersion of 2 mg mL^{-1} concentration was first dropped on arbitrary substrates including leaves, notes, polyimide (PI) films, and even butterfly wings, as shown in Fig. 3. Then, the as-prepared GO film was directly processed in air with the mask-free and programmable laser scribing technology. The laser power varies from low to high, resulting in three distinct regions: the growth, transition, and etch regions. In the growth region, GO is converted to LSG with an increased thickness. In the transition region, both the growth and etching of LSG occurred simultaneously. The final thickness was almost the same as the initial GO thickness. In the etch region, LSG layers were fully etched by the gasification of both oxygen and carbon species caused by a high laser power. This technology is promising for the scalable manufacturing of graphene-based applications. Zhou et al. also found that GO could be etched during the laser cutting of a quartz substrate.[87] However, owing to the thermal gradient mentioned above, only the top GO layers could be etched. Therefore, the substrate may play an important role in laser scribing. The common substrate and application of the LSG device are listed in Table I.

The conductivity of GO is dominated by ionic conductivity, which depends on the humidity of the environment.[96,97] Gao et al. realized a facile and nontoxic laser-patterned rGO–GO–rGO structure, which was used to build electrical

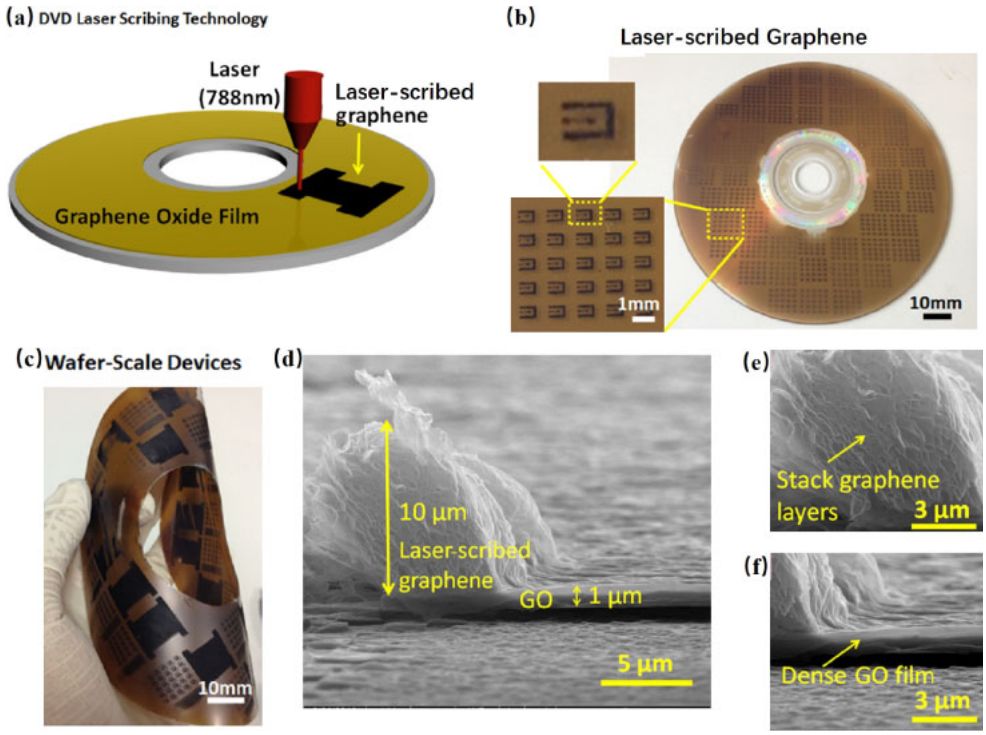

Fig. 2. (Color online) (a) Schematic diagram showing the fabrication process of laser-scribed graphene. A GO film is coated on a DVD media disc. The disc is inserted into a LightScribe DVD drive and a computer-designed circuit is etched onto the film. The laser inside the drive converts the golden-brown GO into black graphene at precise locations. The laser scribing technology makes it possible to obtain large-area precise graphene patterns in 25 min. (b) Image of wafer-scale in-plane transistor patterns produced by laser-scribed graphene. (c) Wafer-scale fabrication flexible graphene-based devices on the PET substrate. (d) Cross-sectional view of GO and laser-scribed graphene film. An increase in laser-scribed graphene film thickness is clearly visible. (e) Zoom-in cross-sectional view of laser-scribed graphene film under high magnification. A stack of graphene layers could be clearly identified. (f) Zoom-in cross-sectional view of GO film under high magnification. Reprinted with permission from Ref. 66. © 2014 Nature Publishing Group.

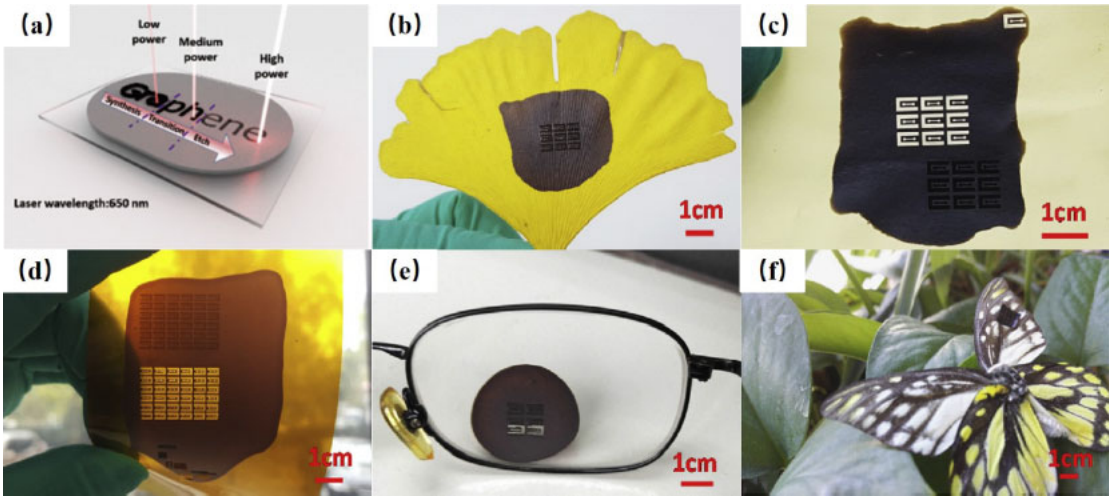

Fig. 3. (Color online) (a) Schematic diagram showing three laser beams irradiating a GO film under three different laser powers. Photographs of grown LSG and etched pattern on arbitrary substrates. These include (b) a piece of ginkgo leaf, (c) a piece of sticky note, (d) polyimide films, (e) a spectacle lens, and (f) a butterfly wing. Reprinted with permission from Ref. 95. © 2016 Elsevier.

double-layer capacitors (EDLCs) or supercapacitors.[85] The ionic conductivity of GO was fully developed, so both in-plane and conventional sandwich structures were designed without an external electrolyte. The in-plane supercapacitor structure with a circular geometry had a capacitance of 0.51 mF cm^{-2}, nearly twice that of the sandwich structure.

2.2 Laser scribing graphene based on polymer

On the basis of laser scribing technology, graphene can also be produced from many types of polymer. Lin et al. developed a method of converting polyimide (PI) films into porous graphene films via one-step laser scribing.[82] Besides PI, LSG can also be produced from poly(ether imide) (PEI). Both of them contain aromatic and imide repeat units. However, LSG was not discovered from other step-growth or chain-growth polymers such as poly(vinyl alcohol) (PVA), poly(methyl methacrylate) (PMMA), PET and many others after laser scribing. Recently, Dorin et al. have demonstrated a one-step laser scribing process for fabricating 3D conductor–

Table I. Substrates for laser scribing graphene.

Substrate	Laser parameter	Carbon source	Resistance	Application	Reference
PET/DVD disc	DVD burner	GO	1738 S/m 8.2 kΩ 2.3 kΩ 2.3 kΩ 2.3 kΩ — 2.3 kΩ 165 Ω/μm	Supercapacitor Earphone Transistor Loudspeaker Photodetector RRAM Press sensor LED	23, 31, 66, 69, 70, 89, 123
PI, silicon wafer, plastic dish, glass lens, PET, cloth, leaf	650 nm	GO	158.7 Ω/□	Heater	45
PDMS	450 nm	GO	— —	Strain sensor Sound source	47, 67, 109
PET	248 nm ns UV pulses 788 nm CW illumination 800 nm 100 fs near IR pulses	GO	—	—	74
Glass, leaf, sticky note, PI, spectacle lens, dress, a butterfly wing	650 nm	GO	763 Ω	Photodetector	95
SiO_2/Si	532 nm	GO	—	—	105
PI	450 nm	PI	—	Intelligent throat	68
PI, PEI	CO_2 IR laser	PI, PEI	25 S/cm	Supercapacitor	82
PDMS	CO_2 IR laser	PI	60 Ω/□	Strain sensor	83
SPEEK	—	SPEEK	—	Supercapacitor	84

insulator composite materials using commercial PI films.[75] The bulk PI was converted into a conductive LSG with a resistivity of 6 $\Omega\,cm^{-1}$. Lamberti et al. developed a method of laser-induced graphenization of sulfonated poly(ether ether ketone) (SPEEK).[84] These approaches are less time-consuming than the laser scribing technique based on GO.

Rahimi et al. converted the PI film into LSG and transferred a patterned LSG onto a poly(dimethylsiloxane) (PDMS) substrate by pouring a diluted form of uncured PDMS over carbon patterns, followed by degassing and cross-linking.[83] The obtained highly porous carbon nano/microparticles have sheet resistances as low as 60 $\Omega\,\square^{-1}$. Owing to the flexibility of PDMS, the strain sensors based on LSG have a strain range of up to 100% and a gauge factor of up to 20000.

2.3 Laser scribing metal technique

Besides graphene, many types of metal can also be directly patterned by a laser scribing technique.[91,98–101] Liu et al. synthesized and patterned a silver film simultaneously on a PI substrate by laser scribing. The resistance of silver patterns fabricated by this method was as low as 2.1 $\mu\Omega\,cm^{-1}$. During laser scribing, elemental silver is formed through two decomposition reactions listed below. The resistance of the patterned film can be adjusted using laser parameters, such as laser power, scribing speed, and the number of times of scribing.[98]

$$2Ag(NH_3)_2CH_3CO_2 + NH_4CO_2 \rightarrow 2Ag + 5NH_3 + 2CH_3CO_2H + CO_2 + H_2O$$

$$2AgCH_3CO_2 + NH_4CO_2 \rightarrow Ag + AgCH_3CO_2 + 5NH_3 + CH_3CO_2H + CO_2 + H_2O$$

Rahimi et al. fabricated porous carbon/silver nanocomposites by direct laser scribing on PI substrates [Figs. 4(a)–4(d)].[99] Zhou et al. developed a new type of silver ink composed of silver nitrate, sodium citrate, and poly(vinyl pyrrolidone) (PVP), which could be patterned by laser scribing [Fig. 4(e)].[101] The silver ink was coated on a flexible polycarbonate (PC) film by scraper coating. After scribing, the substrate was washed with deionized water to remove the sodium ions and unreactive silver ion film. The Ag/C composite lowered the sheet resistance of the original laser-carbonized polyimide from 50 to 0.02 $\Omega\,\square^{-1}$. Huang et al. developed a rapid laser printing technique for fabricating paper-based multilayer circuits based on silver nanowires.[102] A high-frequency (HF) radio frequency identification (RFID) system was realized [Figs. 4(f) and 4(g)].

Copper is commonly used in the CMOS integrated circuit and printed circuit board (PCB). Conventional techniques of fabricating copper typically require expensive equipment, toxic solvents, and complex steps. Zhang et al. successfully prepared high-resolution and metallic circuits on acrylonitrile–butadiene–styrene (ABS) via laser scribing based on $Cu_2(OH)PO_4$.[100] The fabrication of accurate, high-resolution, and well-defined metallic patterns is shown in Figs. 4(h) and 4(i). It is an environmentally friendly and effective strategy for fabricating circuit patterns on a polymer surface, which is a feasible method in the PCB industry. By laser scribing, Zarzar et al. realized the patterns of 13 metal elements (V, Cr, Mn, Fe, Co, Ni, Cu, Mo, Ru, Rh, Pd, Ir, and Pt), as shown in [Figs. 4(j)–4(o)].[91]

2.4 Other laser scribing techniques

Apart from the techniques mentioned above, laser scribing has many other applications in the fabrication of graphene.[103,104] Teoh et al. developed a lift-off technique for

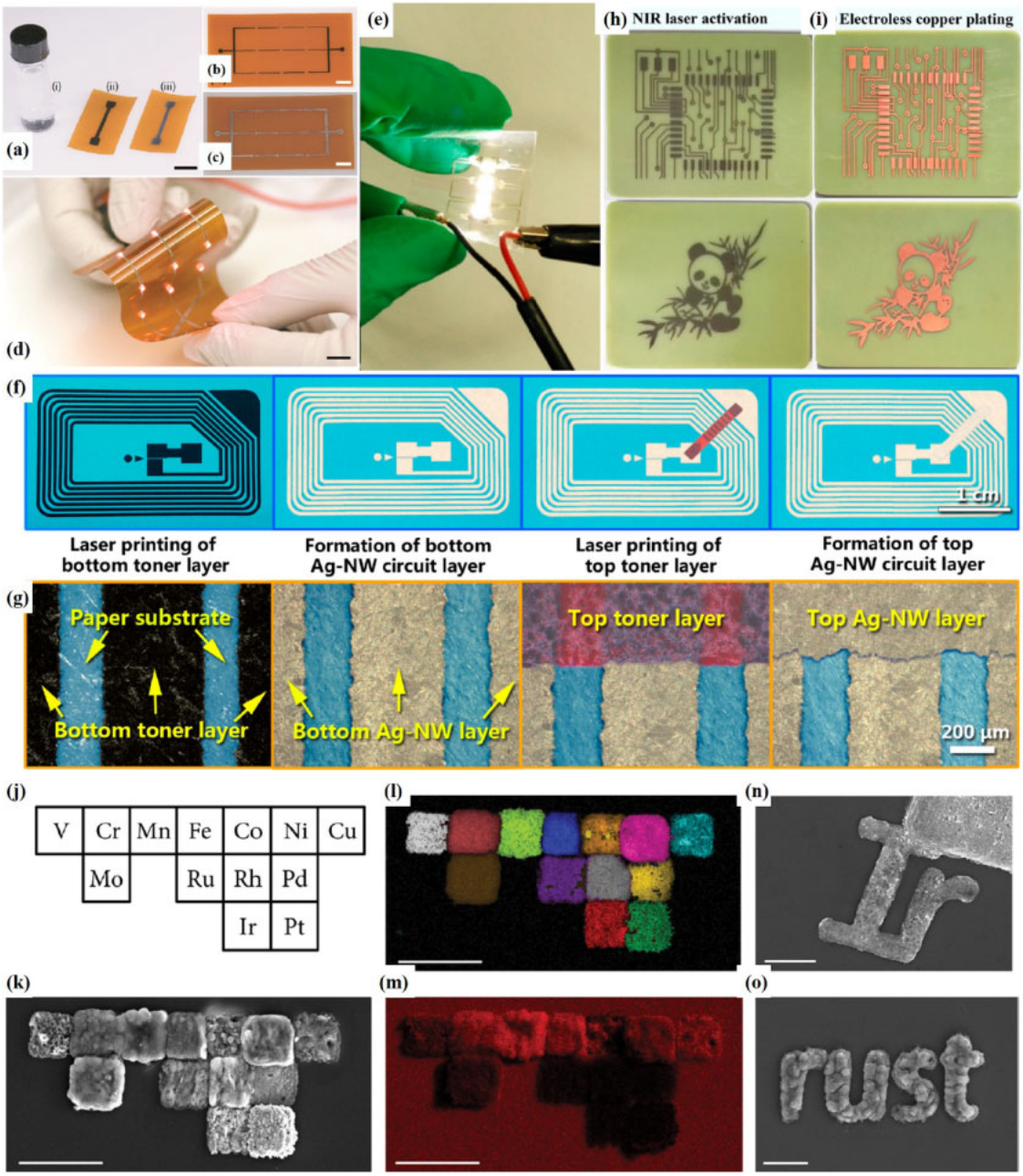

Fig. 4. (Color online) (a) Laser-carbonized traces before and after decorating with silver nanoparticles: (i) silver ionic solution, (ii) pristine carbonized trace, and (iii) carbon/silver nanocomposite. Flexible laser carbonized traces (b) before and (c) after decorating with silver nanoparticles; (d) array of lit LEDs with flexible interconnect. All scale bars = 1 cm. Reprinted with permission from Ref. 99. © 2016 American Chemical Society. (e) Flexible electrodes fabricated by the LDW process for flexible display. The LED glows perfectly after twisting the substrate. Reprinted with permission from Ref. 101. © 2016 American Chemical Society. (f) Digital photographs and (g) optical microscopy images of HF RFID (13.56 MHz) antenna fabricated by the LP method at each processing stage. Reprinted with permission from Ref. 102. © 2016 American Chemical Society. (h) Photographs of the circuit patterns and the panda pattern on the ABS/$Cu_2(OH)PO_4$ composite. After NIR laser activation; (i) after electroless copper plating. Reprinted with permission from Ref. 100. © 2016 American Chemical Society. (j) Target elements and their relative positions in the periodic table are patterned and imaged by (k) scanning electron microscopy and (l, m) energy-dispersive X-ray spectroscopy (EDS). (l) The EDS map directly corresponds to the target elements described in a. (m) The EDS map of oxygen indicates the transition metal oxides (red; oxygen signal) and noble metals (black; little or no oxidation). The scale bar in k–m is 20 μm. (n, o) The mask-directed laser scanning technique enables us to obtain user-defined shapes and patterns, such as the symbol "Ir" (n) written in iridium metal from a solution containing Ir^{3+} ions at the edge of a platinum structure. (o) Word "rust" written in iron oxide (Fe_2O_3) on glass from aqueous potassium ferrate solution. The scale bar in (e) and (f) is 10 μm. Reprinted with permission from Ref. 91. © 2016 American Chemical Society.

patterning GO and rGO.[105] With the aid of a photoresist and an ultrasonic system, either rGO or GO could be preferentially removed by controlling the laser power carefully. Seo et al. found a simple method of doping CVD graphene at specific positions by laser scribing.[106] Graphene mainly showed a p-type doping character in air. 6,13-Bis(triisopropylsilylethynyl) pentacene (TIPS-pentacene) was first spin-casted on top of graphene. After laser scribing, arbitrary shapes of air-stable n-type regions could be created. There are two possible mechanisms to explain the doping character: (1) electron transfer from the photoexcited TIPS-pentacene to graphene and (2) the reaction of graphene with the O_2 anion. Yoo et al. developed a method of transferring and patterning of CVD graphene in a single processing step,[107] which

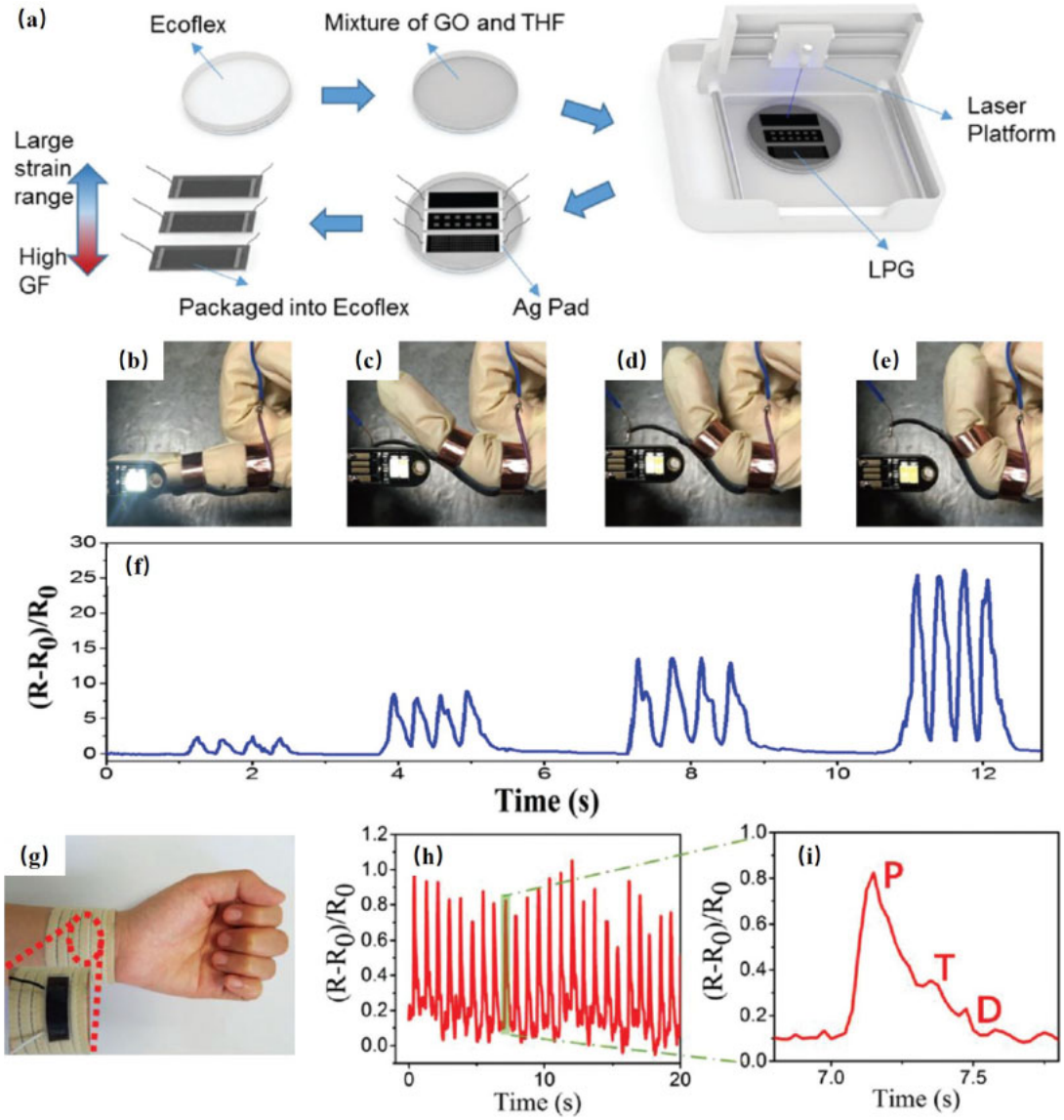

Fig. 5. (Color online) (a) Schematic diagram of the fabrication process of the LPG strain sensors with different mesh densities, realizing the tunable performance by adjusting the mesh densities. (b–e) The brightness of the LED continuously decreases with increasing finger's bending degree. (f) Relative resistance changes at different finger bending degrees. (g) Sensor assembled in a wrist band. (h) Signal induced by wrist pulse. (i) Magnified image of a single pulse, revealing the typical characteristics of the pulse. Reprinted with permission from Ref. 67. © 2017 Royal Society of Chemistry.

minimizes the possibility of graphene contamination due to multiple wet-chemical processes. Cheng et al. fabricated rGO/GO fibers by laser scribing.[108] The rGO/GO fibers with a high tensile strength of up to 100 MPa are flexible enough for arbitrary deformation. The as-prepared rGO/GO fiber rapidly bends from −30 to 140°, when the relative humidity (RH) increases from 10 to 80%.

3. Graphene devices based on laser scribing technology

Owing to the excellent properties of graphene and the high efficiency of laser scribing technology, many LSG devices have been fabricated recently.

3.1 LSG strain sensor

Graphene has a Young's modulus of 1 TPa and an intrinsic strength of 130 GPa,[5] making it an ideal material for strain sensors. However, owing to its ultrathin character, CVD graphene is not suitable for use in strain sensors. Conventional strain sensors rarely have both a high gauge factor and a large strain range. Tao et al. manufactured the sensors based on patterned LSG, which can meet demands in both subtle and large motion situations.[67] The fabrication process is shown in Fig. 5(a). First, an elastic silicone called Ecoflex was chosen as the substrate owing to its ultrahigh stretching ability. Then, a mixture of GO solution and tetrahydrofuran (THF) was dropped on the substrate, and a uniform GO film was left after the volatilization of THF, which is used to realize a whole film. Without THF, the GO film could not be formed uniformly on the Ecoflex surface. To prevent irreparable damage to graphene during stretching, the laser-induced graphene was encapsulated in another layer of Ecoflex. The performance of the strain sensors could be easily tuned by adjusting the patterns of graphene. The high-mesh-density sensor array contained 6×16 meshes; the width of each square mesh is 0.05 cm, which resulted in a higher sensitivity. The strain sensor without a mesh had a larger strain range. Figures 5(b)–5(i) show that LSG strain sensors can be used for gesture detection and control. After

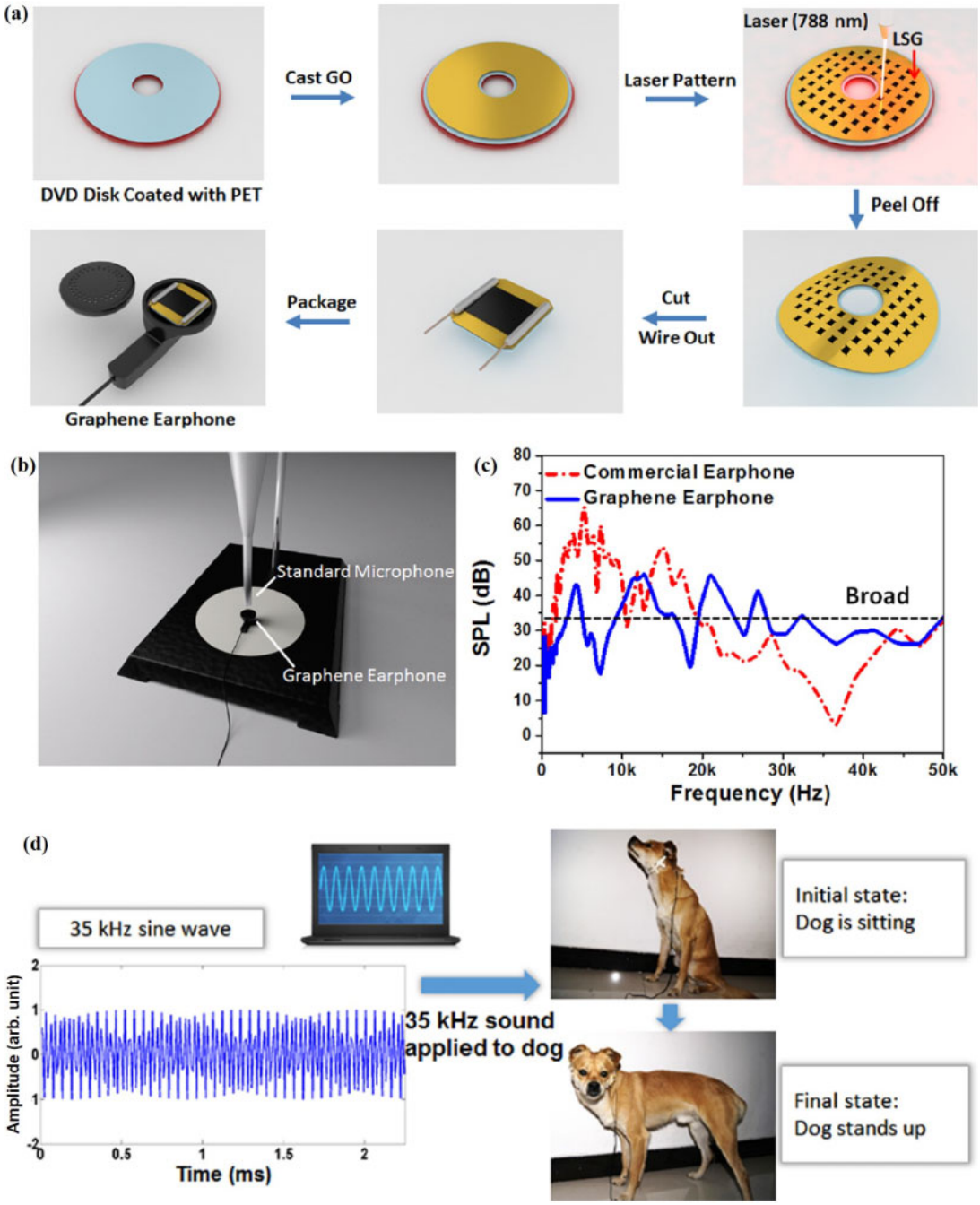

Fig. 6. (Color online) (a) Process flow of the graphene earphone fabrication. (b) Experimental setup for the graphene earphone. (c) Sound pressure level (SPL) curves of a graphene earphone compared with those of a commercial earphone. It is observed that the graphene earphone has a lower fluctuation than a commercial earphone owing to its resonance-free oscillation. (d) Communication with the subject through the earphone in ultrasound. The dog is initially sitting down. After receiving a familiar 35 kHz signal, it stands up. Reprinted with permission from Ref. 69. © 2014 American Chemical Society.

cutting the strain sensors into pieces, they showed an excellent strain range of up to 100% and an ultrahigh GF of 457.

Wang et al. fabricated a self-locked overlapping graphene sheet (SOGS) strain sensor, which achieves good balance between high sensitivity and large strain.[109] The GFs are 34.4 under 2% strain, 99.9 under 5% strain, and 402.3 under 7.5% strain. Owing to its high sensitivity, the SOGS strain sensor can detect various human sounds. The microstructure of graphene comprised SOGS, and the resistance of the sensor was only determined by their overlapping resistance. The overlapping forms of graphene varied under different strains, so their resistances were different. The GFs obtained from the theoretical equation are 33.4 under 2% strain, 85.1 under 5% strain, and up to 387.4 under 7% strain, which are close to the results indicated previously.

3.2 LSG acoustic devices

Graphene has a high thermal conductivity (5300 $W m^{-1} K^{-1}$)[3,4] and a low thermal capacity. The mechanical properties of graphene guarantee tolerance to high-frequency vibrations. Therefore, it is an ideal material for electro-thermoacoustic (ETA) devices. Tian et al. realized wafer-scale graphene earphones by laser-scribing technology.[69] The fabrication process is shown in Fig. 6(a). Short-time laser pulses in a small area of GO may generate oxygen rapidly and increase the layer-to-layer spacing. Therefore,

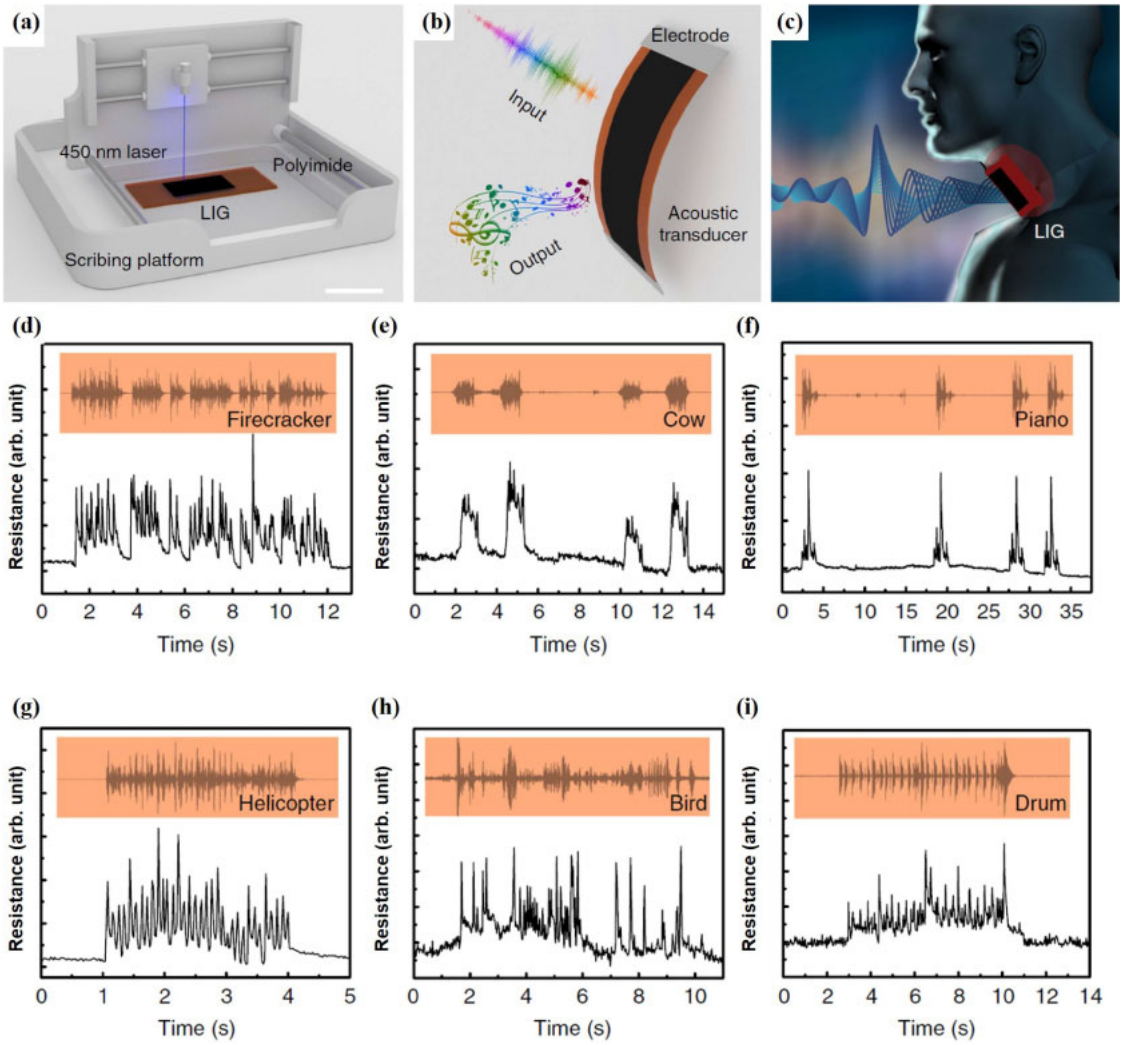

Fig. 7. (Color online) (a) One-step fabrication process of LIG. PI is directly converted into LIG by the irradiation of the 450 nm laser. Scale bar, 2.5 cm. (b) LIG has the ability of emitting and detecting sound in one device. (c) The artificial throat can detect the movement of the human throat and generate a controllable sound. (d) Responses towards different audios from a loudspeaker. The LIG is placed 3 cm away from the loudspeaker. The orange insets above indicate the sound wave profiles of the original audios. Relative resistance changes show responses almost synchronous to profiles of the original audios when the loudspeaker plays the audio of firecrackers, (e) a cow, (f) a piano, (g) a helicopter, (h) a bird, and (i) a drum. Reprinted with permission from Ref. 68.

there are air gaps between graphene layers, which prevent thermal leakage to the substrate. Compared with commercial earphones, LSG earphones exhibit a reasonably flat frequency response and a lower sound pressure fluctuation in a wider frequency range (100 Hz to 50 kHz), as shown in Figs. 6(b) and 6(c). Humans can hear sounds with frequencies ranging from 20 Hz to 20 kHz. However, many animals can communicate in a wider frequency range above 20 kHz in the ultrasonic range. LSG earphones realize communication with a dog through 35 kHz sound waves, which opens up a new way of interspecies communication [Fig. 6(d)].

Apart from the GO thin film, the PI film can be directly converted to graphene by laser scribing.[82] The high thermal conductivity and low heat capacity of LSG are ideal for thermoacoustic sound sources. Moreover, the porous structure has a sensitive response towards weak vibrations, which is suitable for sound detection. However, most rGO strain sensors were encapsulated in an elastic polymer such as Ecoflex[109] or polydimethylsiloxane,[110] which made it impossible to emit Joule heat to the air; thus, they cannot work as sound sources. Tao et al. fabricated an intelligent throat based on laser scribing PI, which can detect and generate sound simultaneously.[68] A custom-designed platform equipped with a laser diode with a wavelength of 450 nm was used to convert PI to LIG. Figure 7(a) shows the schematic diagram of the mask-free process. The movement of the laser was controlled by two stepper motors in the X–Y direction. When the device was attached to the throat, it could detect both SP and throat vibrations, which could clearly differentiate the characteristics of different tones and volumes according to their unique waveforms [Figs. 7(b)–7(i)]. Useful waveforms can be summarized by pattern recognition and machine learning. The intelligent LSG artificial throat will significantly assist a disabled person.

3.3 LSG memory devices

RRAM is a promising candidate for next-generation nonvolatile memory devices, owing to its advantages such as promising scalability, CMOS compatibility, and low cost.[111,112] However, graphene-based memory is usually based on the complex CVD method.[113,114] The substrates are usually rigid. Tian et al. experimentally demonstrated a low-cost, transfer-free, flexible RRAM based on LSG.[70] The

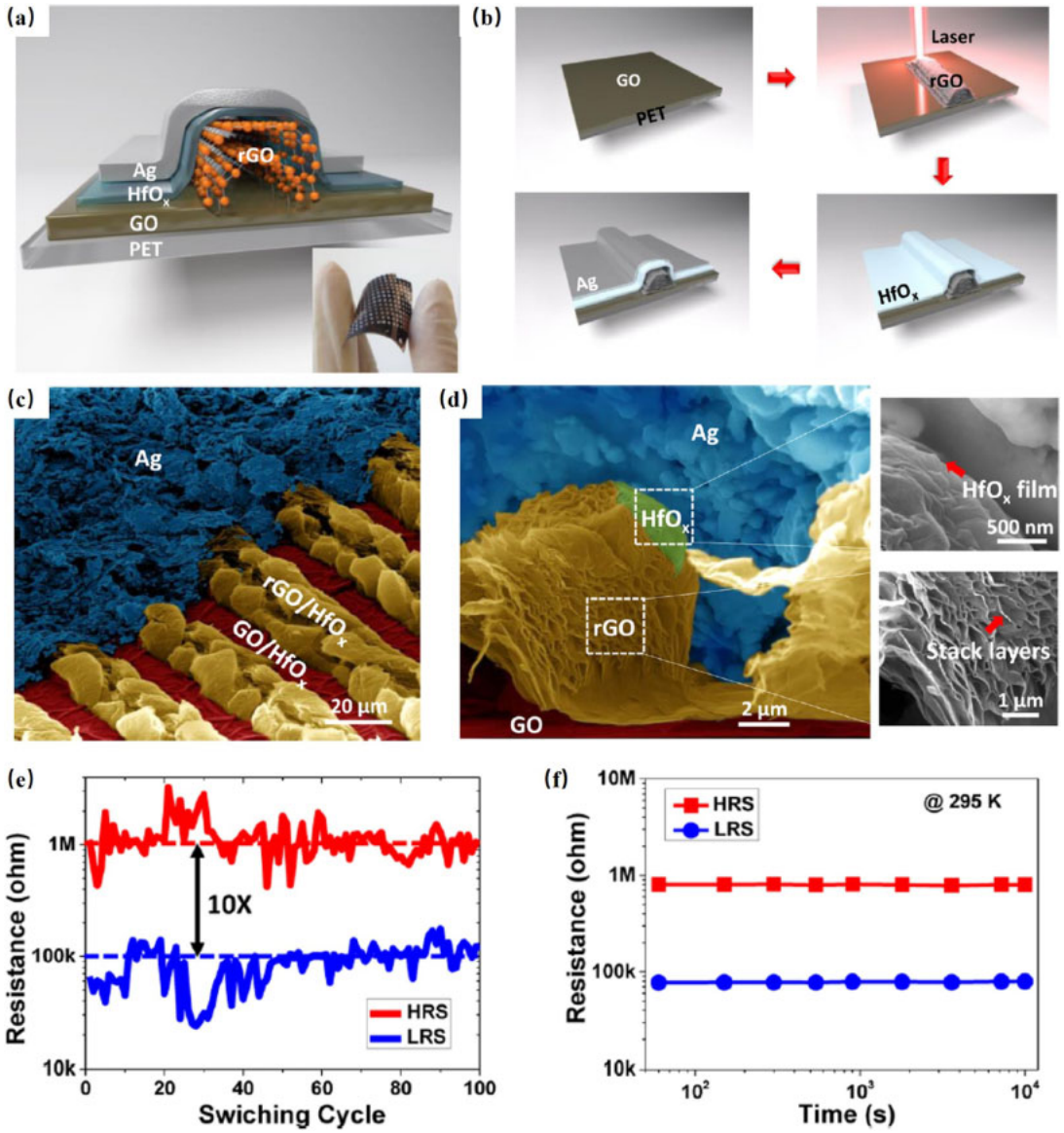

Fig. 8. (Color online) (a) Device structure of the LSG-RRAM. Inset: photo of the fabricated LSG RRAM on a PET substrate. (b) Diagrams showing the main fabrication processing steps of the LSG-RRAM. (c) Top-view SEM image of the LSG-ReRAM in false color. The thickness of HfO_x is 10 nm. The height of the rGO line is 10 μm. (d) Cross-sectional-view SEM image of the LSG-ReRAM. The insets highlight the HfO_x thin film and stacked rGO layers. (e) Dc switching endurance of LSG-ReRAM. (f) Retention measurement of LSG-ReRAM at room temperature. Reprinted with permission from Ref. 70. © 2014 American Chemical Society.

LSG-RRAM was formed by sandwiching Ag/HfO_x/LSG layers, as shown in Figs. 8(a) and 8(b). The thickness of the original GO film on PET was 1 μm. After laser scribing, the LSG was 10 times thicker than the original GO film shown in Figs. 8(c) and 8(d), which appears liked the "Fin" structure in the FinFET.[115] A retention time of up to 10^4 s (equal to ~2.78 h) at 0.1 V reading voltage was achieved with a HRS/LRS ratio of 10 [Figs. 8(e) and 8(f)]. The mechanism of the resistance change entails the formation and breakage of Ag filaments.

3.4 LSG LED

Conventional LEDs are available in different predefined colors whose emission wavelength can only be adjusted by complex material design and bandgap engineering. Some colors must be a combination of primary colors, which needs three devices for only one pixel. The structure of conventional LEDs consists of complex functional layers such as the substrate, anode, hole blocking layer, electron blocking layer, hole injection layer, hole transport layer, emitting layer, electron transport layer, and cathode.[116–118] Wang et al. demonstrated a semi-reduced GO (SRGO) LED by one-step laser scribing, as shown in Fig. 9(a).[23] The light-emitting layer was the interface between GO and rGO, which was a mixture of C–O and C=O bonds. The Fermi and doping levels of SRGO can be modulated either electrically or chemically. The light emission spectrum could be adjusted in situ from blue ($\lambda = 450$ nm) to red ($\lambda = 750$ nm) by electrical gating or environmental doping. Light emission could still be realized even if the device is in the bending state [Figs. 9(b)–9(d)]. The brightness of devices could be up to 6,000 cd m^{-2}, with an efficiency of around 1%. The Poole–Frenkel emission could be used to explain the phenomenon.

3.5 LSG supercapacitors

Supercapacitors are energy devices with ultrahigh power density. Their structure consists of the current collector, electrodes, electrolyte, and separator. Among these, the

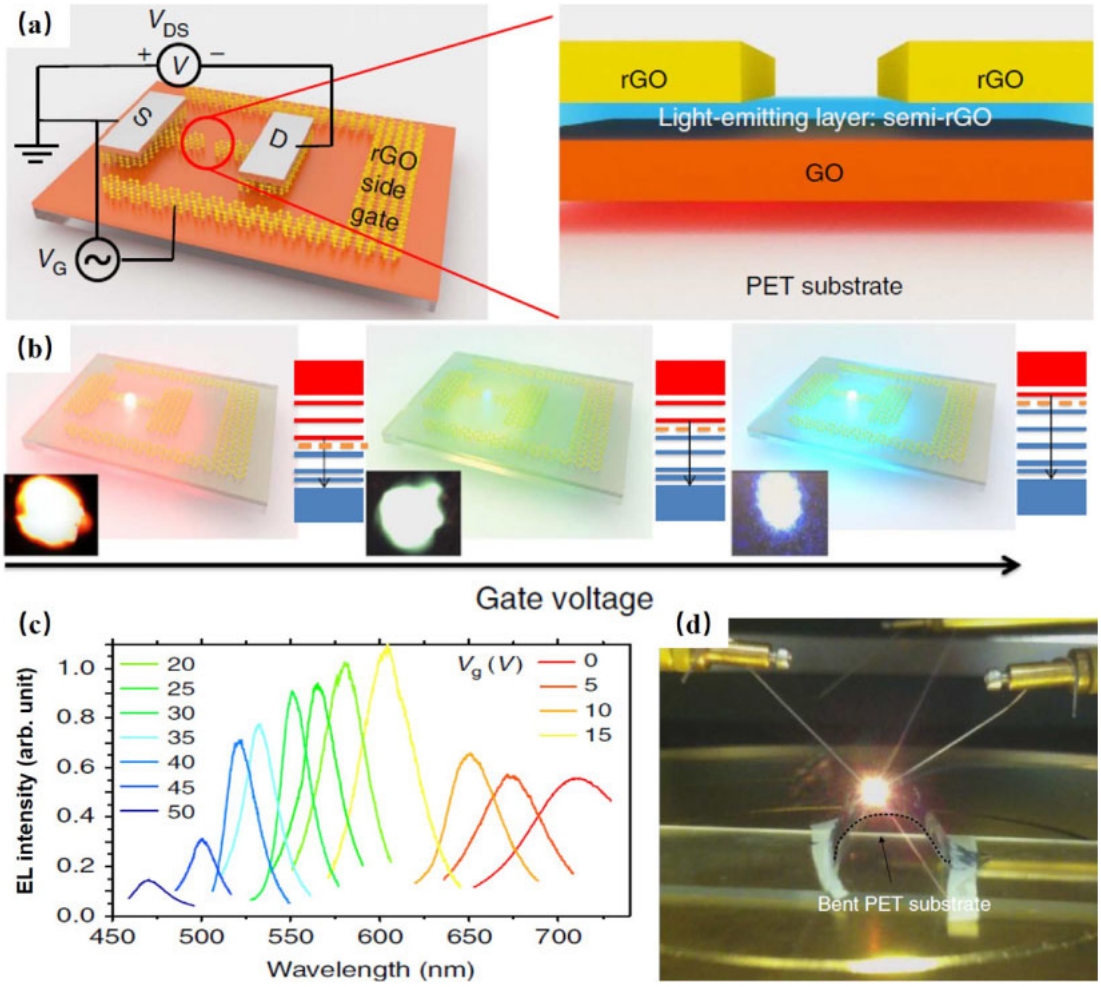

Fig. 9. (Color online) (a) Schematic of the SRGO LED. A distinct semi reduced GO (blue) at the interface between GO (orange) and rGO (gold) is responsible for light emission. (b) Schematic of the gate voltage-dependent EL. The Fermi level determines the lowest unoccupied energy state that mainly participates in the radiative recombination. Inset: corresponding emission images from a real device. (c) Typical EL spectra of a single SRGO LED. Gate biases range from 0 to 50 V. (d) Bright red light emission from the SRGO LED on a flexible PET substrate at a 12 V bias voltage and a 0.1 A drive current. The SRGO LED size is around $100 \times 100\,mm^2$. The edge of the bent PET is marked by a dashed line. The bending radius is around 8 mm. Reprinted with permission from Ref. 23. © 2015 Nature Publishing Group.

electrode are the key to improving device performance. Graphene with a theoretical surface area of $2630\,m^2\,g^{-1}$ is an ideal material for supercapacitors.[119,120] However, the fabrication of on-chip micro-supercapacitors is still an unsolved problem owing to its complexity. In 2012, El-Kady et al. first fabricated supercapacitors by laser scribing.[31] The films produced were mechanically robust with high electrical conductivity ($1738\,S\,m^{-1}$) and specific surface area ($1520\,m^2\,g^{-1}$), which could be used directly as electrodes without binders or current collectors. Then, they took advantage of the laser scribing technique to fabricate rGO interdigital electrodes, which enabled them to obtain on-chip micro-supercapacitor arrays.[89] More supercapacitors have been realized using LSG.[121,122]

4. Challenges and outlook

The system based on LSG consisting of fabrication, patterning, devices, and an integrated system has been basically established. Compared with conventional methods, the fabrication and patterning of graphene can be realized by tuning the power of the laser. However, before the industrialization of graphene, a few problems still need to be solved as listed below. First, the problem regarding a few processes such as alignment between the multistep of laser scribing have not been solved yet. Therefore, it is still difficult to fabricate a multilayer structure by laser scribing technology. Many parameters should be controlled accurately, for example, the thickness of GO thin films. During laser reduction, the rGO line would be wider than the laser spot. Therefore, controlling the width of rGO is another challenge.

Carbon, with tremendous reserves, is naturally inexpensive compared with other elements. Replacing silicon-based integrated circuits with a carbon material has been considered for a long time. However, the high cost of the CVD method limits its development. Graphene produced by laser scribing can keep the main advantages of graphene such as high surface area, electrical conductivity, thermal conductivity, excellent mechanical characteristics and tunable performance. Compared with the CVD method, laser scribing, which is a low-cost and high-efficiency fabrication process, has enormous potential in the industrial application of graphene. This may be a significant breakthrough to make graphene practically applicable. With increasing need for flexible and wearable devices, LSG will have huge market in the future.

5. Conclusions

Laser scribing technology is a low-cost and time-efficient method of producing graphene. The patterning of electronic devices can directly be performed on a large number of substrates using this technology. In this review, the multi-functions of laser scribing technology are discussed. Many devices such as strain sensors, acoustic devices, and RRAM systems based on LSG are introduced. Thus, LSG has great potential for wearable and integrated systems in the future.

Acknowledgments

This work was supported by the National Key R&D Program (2016YFA0200400), National Natural Science Foundation (61574083 and 61434001), National Basic Research Program (2015CB352101), Special Fund for Agroscientific Research in the Public Interest of China (201303107), and Research Fund from Beijing Innovation Center for Future Chip. The authors are also thankful for the support of the Independent Research Program of Tsinghua University (2014Z01006) and Shenzhen Science and Technology Program (JCYJ20150831192224146).

1) K. S. Novoselov, A. K. Geim, S. V. Morozov, D. Jiang, Y. Zhang, S. V. Dubonos, I. V. Grigorieva, and A. A. Firsov, Science **306**, 666 (2004).
2) K. I. Bolotin, K. Sikes, Z. Jiang, M. Klima, G. Fudenberg, J. Hone, P. Kim, and H. Stormer, Solid State Commun. **146**, 351 (2008).
3) A. A. Balandin, S. Ghosh, W. Bao, I. Calizo, D. Teweldebrhan, F. Miao, and C. N. Lau, Nano Lett. **8**, 902 (2008).
4) A. A. Balandin, Nat. Mater. **10**, 569 (2011).
5) C. Lee, X. Wei, J. W. Kysar, and J. Hone, Science **321**, 385 (2008).
6) R. R. Nair, P. Blake, A. N. Grigorenko, K. S. Novoselov, T. J. Booth, T. Stauber, N. M. Peres, and A. K. Geim, Science **320**, 1308 (2008).
7) Y. Zhu, S. Murali, M. D. Stoller, K. Ganesh, W. Cai, P. J. Ferreira, A. Pirkle, R. M. Wallace, K. A. Cychosz, and M. Thommes, Science **332**, 1537 (2011).
8) A. K. Geim and K. S. Novoselov, Nat. Mater. **6**, 183 (2007).
9) A. C. Ferrari, F. Bonaccorso, V. Fal'ko, K. S. Novoselov, S. Roche, P. Boggild, S. Borini, F. H. Koppens, V. Palermo, N. Pugno, J. A. Garrido, R. Sordan, A. Bianco, L. Ballerini, M. Prato, E. Lidorikis, J. Kivioja, C. Marinelli, T. Ryhanen, A. Morpurgo, J. N. Coleman, V. Nicolosi, L. Colombo, A. Fert, M. Garcia-Hernandez, A. Bachtold, G. F. Schneider, F. Guinea, C. Dekker, M. Barbone, Z. Sun, C. Galiotis, A. N. Grigorenko, G. Konstantatos, A. Kis, M. Katsnelson, L. Vandersypen, A. Loiseau, V. Morandi, D. Neumaier, E. Treossi, V. Pellegrini, M. Polini, A. Tredicucci, G. M. Williams, B. H. Hong, J. H. Ahn, J. M. Kim, H. Zirath, B. J. van Wees, H. van der Zant, L. Occhipinti, A. Di Matteo, I. A. Kinloch, T. Seyller, E. Quesnel, X. Feng, K. Teo, N. Rupesinghe, P. Hakonen, S. R. Neil, Q. Tannock, T. Lofwander, and J. Kinaret, Nanoscale **7**, 4598 (2015).
10) F. Schwierz, Nat. Nanotechnol. **5**, 487 (2010).
11) Y. M. Lin, C. Dimitrakopoulos, K. A. Jenkins, D. B. Farmer, H. Y. Chiu, A. Grill, and P. Avouris, Science **327**, 662 (2010).
12) L. Liao, Y. C. Lin, M. Bao, R. Cheng, J. Bai, Y. Liu, Y. Qu, K. L. Wang, Y. Huang, and X. Duan, Nature **467**, 305 (2010).
13) N. Petrone, I. Meric, J. Hone, and K. L. Shepard, Nano Lett. **13**, 121 (2013).
14) F. Xia, T. Mueller, Y. M. Lin, A. Valdes-Garcia, and P. Avouris, Nat. Nanotechnol. **4**, 839 (2009).
15) G. Konstantatos, M. Badioli, L. Gaudreau, J. Osmond, M. Bernechea, F. P. Garcia de Arquer, F. Gatti, and F. H. Koppens, Nat. Nanotechnol. **7**, 363 (2012).
16) F. H. Koppens, T. Mueller, P. Avouris, A. C. Ferrari, M. S. Vitiello, and M. Polini, Nat. Nanotechnol. **9**, 780 (2014).
17) T. Mueller, F. Xia, and P. Avouris, Nat. Photonics **4**, 297 (2010).
18) N. Liu, H. Tian, G. Schwartz, J. B. Tok, T. L. Ren, and Z. Bao, Nano Lett. **14**, 3702 (2014).
19) S. Du, W. Lu, A. Ali, P. Zhao, K. Shehzad, H. Guo, L. Ma, X. Liu, X. Pi, P. Wang, H. Fang, Z. Xu, C. Gao, Y. Dan, P. Tan, H. Wang, C.-T. Lin, J. Yang, S. Dong, Z. Cheng, E. Li, W. Yin, J. Luo, B. Yu, T. Hasan, Y. Xu, W. Hu, and X. Duan, Adv. Mater. **29**, 1700463 (2017).
20) K. Shehzad, T. Shi, A. Qadir, X. Wan, H. Guo, A. Ali, W. Xuan, H. Xu, Z. Gu, X. Peng, J. Xie, L. Sun, Q. He, Z. Xu, C. Gao, Y. S. Rim, Y. Dan, T. Hasan, P. Tan, E. Li, W. Yin, Z. Cheng, B. Yu, Y. Xu, J. Luo, and X. Duan, Adv. Mater. Technol. **2**, 1600262 (2017).
21) X. Wan, Y. Xu, H. Guo, K. Shehzad, A. Ali, Y. Liu, J. Yang, D. Dai, C.-T. Lin, L. Liu, H.-C. Cheng, F. Wang, X. Wang, H. Lu, W. Hu, X. Pi, Y. Dan, J. Luo, T. Hasan, X. Duan, X. Li, J. Xu, D. Yang, T. Ren, and B. Yu, 2D Mater. Appl. **1**, 4 (2017).
22) Y. Xu, A. Ali, K. Shehzad, N. Meng, M. Xu, Y. Zhang, X. Wang, C. Jin, H. Wang, Y. Guo, Z. Yang, B. Yu, Y. Liu, Q. He, X. Duan, X. Wang, P. H. Tan, W. Hu, H. Lu, and T. Hasan, Adv. Mater. Technol. **2**, 1600241 (2017).
23) X. Wang, H. Tian, M. A. Mohammad, C. Li, C. Wu, Y. Yang, and T. L. Ren, Nat. Commun. **6**, 7767 (2015).
24) D. I. Son, B. W. Kwon, D. H. Park, W. S. Seo, Y. Yi, B. Angadi, C. L. Lee, and W. K. Choi, Nat. Nanotechnol. **7**, 465 (2012).
25) T. H. Han, Y. Lee, M. R. Choi, S. H. Woo, S. H. Bae, B. H. Hong, J. H. Ahn, and T. W. Lee, Nat. Photonics **6**, 105 (2012).
26) J. T. Seo, J. Han, T. Lim, K. H. Lee, J. Hwang, H. Yang, and S. Ju, ACS Nano **8**, 12476 (2014).
27) S. Bae, H. Kim, Y. Lee, X. Xu, J. S. Park, Y. Zheng, J. Balakrishnan, T. Lei, H. R. Kim, Y. I. Song, Y. J. Kim, K. S. Kim, B. Ozyilmaz, J. H. Ahn, B. H. Hong, and S. Iijima, Nat. Nanotechnol. **5**, 574 (2010).
28) K. S. Kim, Y. Zhao, H. Jang, S. Y. Lee, J. M. Kim, K. S. Kim, J.-H. Ahn, P. Kim, J. Y. Choi, and B. H. Hong, Nature **457**, 706 (2009).
29) H. Wang, Y. Yang, Y. Liang, L. F. Cui, H. S. Casalongue, Y. Li, G. Hong, Y. Cui, and H. Dai, Angew. Chem., Int. Ed. **50**, 7364 (2011).
30) Z. S. Wu, W. Ren, L. Wen, L. Gao, J. Zhao, Z. Chen, G. Zhou, F. Li, and H. M. Cheng, ACS Nano **4**, 3187 (2010).
31) M. F. El-Kady, V. Strong, S. Dubin, and R. B. Kaner, Science **335**, 1326 (2012).
32) L. Q. Tao, D. Y. Wang, H. Tian, Z. Y. Ju, Y. Liu, Y. Q. Chen, Q. Y. Xie, H. M. Zhao, Y. Yang, and T. L. Ren, IEDM Tech. Dig., 2017, 18.3.1.
33) Y. Pang, H. Tian, L. Tao, Y. Li, X. Wang, N. Deng, Y. Yang, and T. L. Ren, ACS Appl. Mater. Interfaces **8**, 26458 (2016).
34) Y. Shu, H. Tian, Y. Yang, C. Li, Y. Cui, W. Mi, Y. Li, Z. Wang, N. Deng, B. Peng, and T. L. Ren, Nanoscale **7**, 8636 (2015).
35) V. Strong, S. Dubin, M. F. El-Kady, A. Lech, Y. Wang, B. H. Weiller, and R. B. Kaner, ACS Nano **6**, 1395 (2012).
36) F. Schedin, A. K. Geim, S. V. Morozov, E. W. Hill, P. Blake, M. I. Katsnelson, and K. S. Novoselov, Nat. Mater. **6**, 652 (2007).
37) H. Tian, H. Zhao, X. F. Wang, Q. Y. Xie, H. Y. Chen, M. A. Mohammad, C. Li, W. T. Mi, Z. Bie, C. H. Yeh, Y. Yang, H. S. Wong, P. W. Chiu, and T. L. Ren, Adv. Mater. **27**, 7767 (2015).
38) H. Tian, H. Y. Chen, B. Gao, S. Yu, J. Liang, Y. Yang, D. Xie, J. Kang, T. L. Ren, Y. Zhang, and H. S. Wong, Nano Lett. **13**, 651 (2013).
39) C. He, Z. Shi, L. Zhang, W. Yang, R. Yang, D. Shi, and G. Zhang, ACS Nano **6**, 4214 (2012).
40) X. F. Wang, H. M. Zhao, Y. Yang, and T. L. Ren, Chin. Phys. B **26**, 038501 (2017).
41) H. Tian, S. Ma, H. M. Zhao, C. Wu, J. Ge, D. Xie, Y. Yang, and T. L. Ren, Nanoscale **5**, 8951 (2013).
42) D. Choi, M. Y. Choi, W. M. Choi, H. J. Shin, H. K. Park, J. S. Seo, J. Park, S. M. Yoon, S. J. Chae, Y. H. Lee, S. W. Kim, J. Y. Choi, S. Y. Lee, and J. M. Kim, Adv. Mater. **22**, 2187 (2010).
43) T. Y. Zhang, H. M. Zhao, D. Y. Wang, Q. Wang, Y. Pang, N. Q. Deng, H. W. Cao, Y. Yang, and T. L. Ren, Nanoscale **9**, 14357 (2017).
44) T. Y. Zhang, H. M. Zhao, Z. Yang, Q. Wang, D. Y. Wang, N. Q. Deng, Y. Yang, and T. L. Ren, Appl. Phys. Lett. **109**, 151905 (2016).
45) S. Y. Lin, T. Y. Zhang, Q. Lu, D. Y. Wang, Y. Yang, X. M. Wu, and T. L. Ren, RSC Adv. **7**, 27001 (2017).
46) H. Tian, T. L. Ren, D. Xie, Y. F. Wang, C. J. Zhou, T. T. Feng, D. Fu, Y. Yang, P. G. Peng, and L. G. Wang, ACS Nano **5**, 4878 (2011).
47) L.-Q. Tao, Y. Liu, Z.-Y. Ju, H. Tian, Q.-Y. Xie, Y. Yang, and T.-L. Ren, Nanomaterials **6**, 112 (2016).
48) H. Tian, Y. Yang, D. Xie, J. Ge, and T. L. Ren, RSC Adv. **3**, 17672 (2013).
49) H. Tian, D. Xie, Y. Yang, T. L. Ren, Y. F. Wang, C. J. Zhou, P. G. Peng, L. G. Wang, and L. T. Liu, Nanoscale **4**, 2272 (2012).
50) F. Xia, H. Wang, D. Xiao, M. Dubey, and A. Ramasubramaniam, Nat. Photonics **8**, 899 (2014).
51) I. Meric, C. R. Dean, N. Petrone, L. Wang, J. Hone, P. Kim, and K. L. Shepard, Proc. IEEE **101**, 1609 (2013).
52) C. R. Dean, A. F. Young, I. Meric, C. Lee, L. Wang, S. Sorgenfrei, K. Watanabe, T. Taniguchi, P. Kim, K. L. Shepard, and J. Hone, Nat. Nanotechnol. **5**, 722 (2010).

53) G. Hu, T. Albrow-Owen, X. Jin, A. Ali, Y. Hu, R. C. T. Howe, K. Shehzad, Z. Yang, X. Zhu, R. I. Woodward, T. C. Wu, H. Jussila, J. B. Wu, P. Peng, P. H. Tan, Z. Sun, E. J. R. Kelleher, M. Zhang, Y. Xu, and T. Hasan, Nat. Commun. **8**, 278 (2017).
54) H. S. Lee, S. W. Min, Y. G. Chang, M. K. Park, T. Nam, H. Kim, J. H. Kim, S. Ryu, and S. Im, Nano Lett. **12**, 3695 (2012).
55) L. Li, Y. Yu, G. J. Ye, Q. Ge, X. Ou, H. Wu, D. Feng, X. H. Chen, and Y. Zhang, Nat. Nanotechnol. **9**, 372 (2014).
56) S. B. Desai, S. R. Madhvapathy, A. B. Sachid, J. P. Llinas, Q. Wang, G. H. Ahn, G. Pitner, M. J. Kim, J. Bokor, and C. Hu, Science **354**, 99 (2016).
57) X. Xu, Z. Zhang, J. Dong, D. Yi, J. Niu, M. Wu, L. Lin, R. Yin, M. Li, J. Zhou, S. Wang, J. Sun, X. Duan, P. Gao, Y. Jiang, X. Wu, H. Peng, R. S. Ruoff, Z. Liu, D. Yu, E. Wang, F. Ding, and K. Liu, Sci. Bull. **62**, 1074 (2017).
58) Y. Zhu, S. Murali, W. Cai, X. Li, J. W. Suk, J. R. Potts, and R. S. Ruoff, Adv. Mater. **22**, 3906 (2010).
59) L. Q. Tao, K. N. Zhang, H. Tian, Y. Liu, D. Y. Wang, Y. Q. Chen, Y. Yang, and T. L. Ren, ACS Nano **11**, 8790 (2017).
60) D. Yang, A. Velamakanni, G. Bozoklu, S. Park, M. Stoller, R. D. Piner, S. Stankovich, I. Jung, D. A. Field, C. A. Ventrice, and R. S. Ruoff, Carbon **47**, 145 (2009).
61) D. Li, M. B. Muller, S. Gilje, R. B. Kaner, and G. G. Wallace, Nat. Nanotechnol. **3**, 101 (2008).
62) V. C. Tung, M. J. Allen, Y. Yang, and R. B. Kaner, Nat. Nanotechnol. **4**, 25 (2009).
63) L. J. Cote, R. Cruzsilva, and J. Huang, J. Am. Chem. Soc. **131**, 11027 (2009).
64) V. Abdelsayed, S. Moussa, H. M. Hassan, H. S. Aluri, M. M. Collinson, and M. S. El-Shall, J. Phys. Chem. Lett. **1**, 2804 (2010).
65) L. Tao, D. Wang, S. Jiang, Y. Liu, Q. Xie, H. Tian, N. Deng, X. Wang, Y. Yang, and T.-L. Ren, J. Semicond. **37**, 041001 (2016).
66) H. Tian, Y. Yang, D. Xie, Y.-L. Cui, W.-T. Mi, Y. Zhang, and T.-L. Ren, Sci. Rep. **4**, 3598 (2014).
67) L. Q. Tao, D. Y. Wang, H. Tian, Z. Y. Ju, Y. Liu, Y. Pang, Y. Q. Chen, Y. Yang, and T. L. Ren, Nanoscale **9**, 8266 (2017).
68) L. Q. Tao, H. Tian, Y. Liu, Z. Y. Ju, Y. Pang, Y. Q. Chen, D. Y. Wang, X. G. Tian, J. C. Yan, N. Q. Deng, Y. Yang, and T. L. Ren, Nat. Commun. **8**, 14579 (2017).
69) H. Tian, C. Li, M. A. Mohammad, Y. L. Cui, W. T. Mi, Y. Yang, D. Xie, and T. L. Ren, ACS Nano **8**, 5883 (2014).
70) H. Tian, H. Y. Chen, T. L. Ren, C. Li, Q. T. Xue, M. A. Mohammad, C. Wu, Y. Yang, and H. S. Wong, Nano Lett. **14**, 3214 (2014).
71) Z. Wei, D. Wang, S. Kim, S. Y. Kim, Y. Hu, M. K. Yakes, A. R. Laracuente, Z. Dai, S. R. Marder, and C. Berger, Science **328**, 1373 (2010).
72) A. Einstein, Phys. Z. **18**, 121 (1917) [in German].
73) Y. Zhang, L. Guo, S. Wei, Y. He, H. Xia, Q. Chen, H. B. Sun, and F. S. Xiao, Nano Today **5**, 15 (2010).
74) R. Arul, R. N. Oosterbeek, J. Robertson, G. Xu, J. Jin, and M. C. Simpson, Carbon **99**, 423 (2016).
75) B. Dorin, P. Parkinson, and P. Scully, J. Mater. Chem. C **5**, 4923 (2017).
76) M. Qian, Y. S. Zhou, Y. Gao, J. B. Park, T. Feng, S. M. Huang, Z. Sun, L. Jiang, and Y. F. Lu, Appl. Phys. Lett. **98**, 173108 (2011).
77) A. Longo, R. Verucchi, L. Aversa, R. Tatti, A. Ambrosio, E. Orabona, U. Coscia, G. Carotenuto, and P. Maddalena, Nanotechnology **28**, 224002 (2017).
78) S. Lee, M. F. Toney, W. Ko, J. C. Randel, H. J. Jung, K. Munakata, J. Lu, T. H. Geballe, M. R. Beasley, and R. Sinclair, ACS Nano **4**, 7524 (2010).
79) K. Wang, G. Tai, K. H. Wong, S. P. Lau, and W. Guo, AIP Adv. **1**, 022141 (2011).
80) A. T. T. Koh, Y. M. Foong, and D. H. C. Chua, Appl. Phys. Lett. **97**, 114102 (2010).
81) S. Luo, P. T. Hoang, and T. Liu, Carbon **96**, 522 (2016).
82) J. Lin, Z. Peng, Y. Liu, F. Ruiz-Zepeda, R. Ye, E. L. Samuel, M. J. Yacaman, B. I. Yakobson, and J. M. Tour, Nat. Commun. **5**, 5714 (2014).
83) R. Rahimi, M. Ochoa, W. Yu, and B. Ziaie, ACS Appl. Mater. Interfaces **7**, 4463 (2015).
84) A. Lamberti, M. Serrapede, G. Ferraro, M. Fontana, F. Perrucci, S. Bianco, A. Chiolerio, and S. Bocchini, 2D Mater. **4**, 035012 (2017).
85) W. Gao, N. Singh, L. Song, Z. Liu, A. L. Reddy, L. Ci, R. Vajtai, Q. Zhang, B. Wei, and P. M. Ajayan, Nat. Nanotechnol. **6**, 496 (2011).
86) X. Ye, J. Long, Z. Lin, H. Zhang, H. Zhu, and M. Zhong, Carbon **68**, 784 (2014).
87) Y. Zhou, Q. Bao, B. Varghese, L. A. Tang, C. K. Tan, C. H. Sow, and K. P. Loh, Adv. Mater. **22**, 67 (2010).
88) F. Cai, C. A. Tao, Y. Li, W. Yin, X. Wang, and J. Wang, Mater. Res. Express **4**, 036304 (2017).
89) M. F. El-Kady and R. B. Kaner, Nat. Commun. **4**, 1475 (2013).
90) Y. Zhao, Q. Han, Z. Cheng, L. Jiang, and L. Qu, Nano Today **12**, 14 (2017).
91) L. D. Zarzar, B. S. Swartzentruber, B. F. Donovan, P. E. Hopkins, and B. Kaehr, ACS Appl. Mater. Interfaces **8**, 21134 (2016).
92) K. Shehzad, Y. Xu, C. Gao, and X. Duan, Chem. Soc. Rev. **45**, 5541 (2016).
93) W. S. Hummers, Jr. and R. E. Offeman, J. Am. Chem. Soc. **80**, 1339 (1958).
94) A. Furio, G. Landi, C. Altavilla, D. Sofia, S. Iannace, A. Sorrentino, and H. C. Neitzert, Nanotechnology **28**, 054003 (2017).
95) N. Q. Deng, H. Tian, Z. Y. Ju, H. M. Zhao, C. Li, M. A. Mohammad, L. Q. Tao, Y. Pang, X. F. Wang, T. Y. Zhang, Y. Yang, and T. L. Ren, Carbon **109**, 173 (2016).
96) W. Gao, L. B. Alemany, L. Ci, and P. M. Ajayan, Nat. Chem. **1**, 403 (2009).
97) S. Park, J. An, R. D. Piner, I. Jung, D. Yang, A. Velamakanni, S. T. Nguyen, and R. S. Ruoff, Chem. Mater. **20**, 6592 (2008).
98) Y. K. Liu and M. T. Lee, ACS Appl. Mater. Interfaces **6**, 14576 (2014).
99) R. Rahimi, M. Ochoa, and B. Ziaie, ACS Appl. Mater. Interfaces **8**, 16907 (2016).
100) J. Zhang, T. Zhou, L. Wen, and A. Zhang, ACS Appl. Mater. Interfaces **8**, 33999 (2016).
101) W. Zhou, S. Bai, Y. Ma, D. Ma, T. Hou, X. Shi, and A. Hu, ACS Appl. Mater. Interfaces **8**, 24887 (2016).
102) G. W. Huang, Q. P. Feng, H. M. Xiao, N. Li, and S. Y. Fu, ACS Nano **10**, 8895 (2016).
103) M. F. El-Kady and R. B. Kaner, ACS Nano **8**, 8725 (2014).
104) A. M. Pérez-Mas, P. Álvarez, N. Campos, D. Gómez, and R. Menéndez, J. Phys. D **49**, 305301 (2016).
105) H. F. Teoh, Y. Tao, E. S. Tok, G. W. Ho, and C. H. Sow, J. Appl. Phys. **112**, 064309 (2012).
106) B. H. Seo, J. Youn, and M. Shim, ACS Nano **8**, 8831 (2014).
107) J. H. Yoo, J. B. Park, S. Ahn, and C. P. Grigoropoulos, Small **9**, 4269 (2013).
108) H. Cheng, J. Liu, Y. Zhao, C. Hu, Z. Zhang, N. Chen, L. Jiang, and L. Qu, Angew. Chem., Int. Ed. **52**, 10482 (2013).
109) D. Y. Wang, L. Q. Tao, Y. Liu, T. Y. Zhang, Y. Pang, Q. Wang, S. Jiang, Y. Yang, and T. L. Ren, Nanoscale **8**, 20090 (2016).
110) J. J. Park, W. J. Hyun, S. C. Mun, Y. T. Park, and O. O. Park, ACS Appl. Mater. Interfaces **7**, 6317 (2015).
111) A. Chen, Solid-State Electron. **125**, 25 (2016).
112) M. Di Ventra and Y. V. Pershin, Mater. Today **14** [12], 584 (2011).
113) A. J. Hong, E. B. Song, H. S. Yu, M. J. Allen, J. Kim, J. D. Fowler, J. K. Wassei, Y. Park, Y. Wang, and J. Zou, ACS Nano **5**, 7812 (2011).
114) J. Yao, J. Lin, Y. Dai, G. Ruan, Z. Yan, L. Li, L. Zhong, D. Natelson, and J. M. Tour, Nat. Commun. **3**, 1101 (2012).
115) D. Hisamoto, W.-C. Lee, J. Kedzierski, H. Takeuchi, K. Asano, C. Kuo, E. Anderson, T.-J. King, J. Bokor, and C. Hu, IEEE Trans. Electron Devices **47**, 2320 (2000).
116) Y. Shirasaki, G. J. Supran, M. G. Bawendi, and V. Bulović, Nat. Photonics **7**, 13 (2013).
117) J. M. Caruge, J. E. Halpert, V. Wood, V. Bulović, and M. G. Bawendi, Nat. Photonics **2**, 247 (2008).
118) X. Dai, Z. Zhang, Y. Jin, Y. Niu, H. Cao, X. Liang, L. Chen, J. Wang, and X. Peng, Nature **515**, 96 (2014).
119) M. D. Stoller, S. Park, Y. Zhu, J. An, and R. S. Ruoff, Nano Lett. **8**, 3498 (2008).
120) C. Liu, Z. Yu, D. Neff, A. Zhamu, and B. Z. Jang, Nano Lett. **10**, 4863 (2010).
121) B. Xie, Y. Wang, W. Lai, W. Lin, Z. Lin, Z. Zhang, P. Zou, Y. Xu, S. Zhou, C. Yang, F. Kang, and C. P. Wong, Nano Energy **26**, 276 (2016).
122) F. Wen, C. Hao, J. Xiang, L. Wang, H. Hou, Z. Su, W. Hu, and Z. Liu, Carbon **75**, 236 (2014).
123) H. Tian, Y. Shu, X. F. Wang, M. A. Mohammad, Z. Bie, Q. Y. Xie, C. Li, W. T. Mi, Y. Yang, and T. L. Ren, Sci. Rep. **5**, 8603 (2015).